
Non-approximate Inference for Collective Graphical Models on Path Graphs via Discrete Difference of Convex Algorithm

Yasunori Akagi¹ Naoki Marumo² Hideaki Kim¹ Takeshi Kurashima¹ Hiroyuki Toda¹

Abstract

The importance of aggregated count data, which is calculated from the data of multiple individuals, continues to increase. Collective Graphical Model (CGM) is a probabilistic approach to the analysis of aggregated data. One of the most important operations in CGM is maximum a posteriori (MAP) inference of unobserved variables under given observations. Because the MAP inference problem for general CGMs has been shown to be NP-hard, an approach that solves an approximate problem has been proposed. However, this approach has two major drawbacks. First, the quality of the solution deteriorates when the values in the count tables are small, because the approximation becomes inaccurate. Second, since continuous relaxation is applied, the integrality constraints of the output are violated. To resolve these problems, this paper proposes a new method for MAP inference for CGMs on path graphs. First we show that the MAP inference problem can be formulated as a (non-linear) minimum cost flow problem. Then, we apply Difference of Convex Algorithm (DCA), which is a general methodology to minimize a function represented as the sum of a convex function and a concave function. In our algorithm, important subroutines in DCA can be efficiently calculated by minimum convex cost flow algorithms. Experiments show that the proposed method outputs higher quality solutions than the conventional approach.

1. Introduction

In recent years, the importance of aggregated count data, which is calculated from the data of multiple individuals, has been increasing (Tanaka et al., 2019; Zhang et al., 2020). Although technologies for acquiring individual data such

as sensors and GPS have greatly advanced, it is still very difficult to handle individual data due to privacy concerns and the difficulty of tracking individuals. However, there are many situations where data aggregated from multiple individuals can be obtained and utilized easily. For example, Mobile Spatial Statistics (Terada et al., 2013), which is the hourly population data of fixed-size square grids calculated from cell phone network data in Japan, are available for purchase; such data is being used for disaster prevention and urban planning (Suzuki et al., 2013). In traffic networks, traffic volume data at each point can be obtained more easily by sensors or cameras than the trajectories of individual cars, and the data is useful for managing traffic congestion (Morimura et al., 2013; Zhang et al., 2017).

Collective Graphical Model (CGM) (Sheldon & Dietterich, 2011) is a probabilistic model to describe aggregated statistics of multiple samples drawn from a graphical model. CGM makes it possible to conduct various practical tasks on aggregate count data, such as estimating movements from population snapshots, parameter learning, interpolation and denoising of count tables. In this paper, we focus on the case where the underlying graphical model is on a path graph. CGMs on path graphs are particularly important because they treat time series data in which the states of interest follow Markov chains. In fact, most of the real-world applications of CGMs utilize CGMs on path graphs to represent the collective movement of humans and animals (Du et al., 2014; Sun et al., 2015; Akagi et al., 2018).

One of the most important operations in CGM is maximum a posteriori (MAP) inference. MAP inference is the discrete (combinatorial) optimization problem of finding an assignment of unobserved variables that maximizes posterior probability under given observations. MAP inference makes it possible to interpolate missing values of aggregated data and to estimate more detailed information that lies behind the observations. Unfortunately, MAP inference for general CGMs has been shown to be NP-hard (Sheldon et al., 2013) and thus is difficult to solve exactly and efficiently. Therefore, an alternative approach that solves an approximate problem, which is derived by applying Stirling's approximation and continuous relaxation, has been proposed (Sheldon et al., 2013). Subsequent studies have fo-

¹NTT Service Evolution Laboratories ²NTT Communication Science Laboratories. Correspondence to: Yasunori Akagi <yasunori.akagi.cu@hco.ntt.co.jp>.

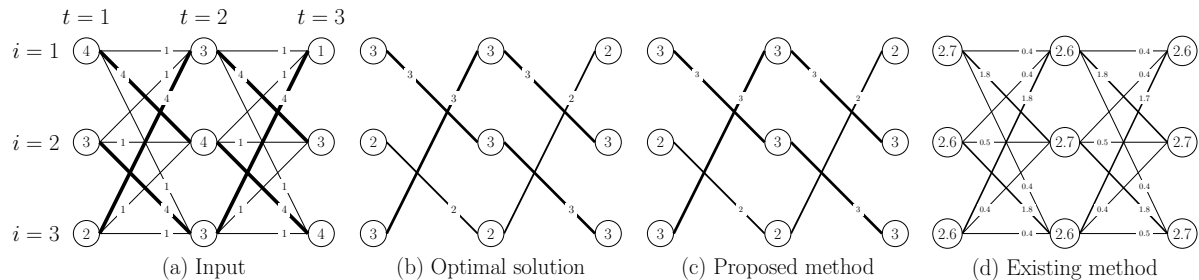


Figure 1. Comparison of MAP inference results obtained by the proposed method and the existing method. (a) Input of the MAP inference problem. The values written in nodes are observations and the values written on edges are potentials. As the noise distribution, we use Gaussian distribution. (b) An optimal solution obtained by brute force search. Note that brute force search is possible only when input size is extremely small. (c) The output of the proposed method. (d) The output of the existing method, non-linear belief propagation (Sun et al., 2015). The values written in nodes are node count table values and the values written on edges are edge count table values. The total population is set to be 8 in all methods. As we can see, the proposed method outputs integer-valued and sparse optimal solutions while the existing method does not.

cused on solving this approximate problem efficiently (Sun et al., 2015; Vilnis et al., 2015; Nguyen et al., 2016; Singh et al., 2020).

However, there are inherent problems with this approach of solving the approximate problem. First, this approach tends to output a solution with low posterior probability when the values in the count tables are small, because Stirling’s approximation, $\log x! \approx x \log x - x$, is inaccurate when x is small. This situation frequently occurs when the number of values that each variable in the graphical model takes is large, or when the total population is small. Second, since continuous relaxation is applied, the integrality constraints of count table values are violated in the output. As a result, values that should be integers (e.g., the number of people) are no longer integers, which not only reduces interpretability, but also makes the output less sparse, resulting in high memory consumption to maintain the output. It is possible to obtain integer-valued results by rounding output, but this rounding process destroys the consistency of the counts among the aggregated data. For example, the sum of the count table values at each node may not match the total population.

In this paper, we propose a new method for MAP inference for CGMs on path graphs to resolve these issues. First, we show that the problem can be formulated as a combinatorial optimization problem called the (nonlinear) minimum cost flow problem (MCFP). MCFP is known to be an optimization problem with good properties and can be solved efficiently when the cost function on each edge satisfies the discrete convex conditions (Ahuja et al., 1993). However, the MCFP in our settings is difficult to solve, because the cost functions of several edges do not satisfy the discrete convex condition. To deal with this, we utilize the Difference of Convex Algorithm (DCA) (Le Thi & Dinh, 2018). DCA is a framework to minimize a function expressed as the

sum of a convex function and a concave function. A solution is obtained by repeatedly minimizing a surrogate function that upper-bounds the objective function. We show that in our problem, the surrogate function can be easily computed in closed form, and that the surrogate function can be minimized efficiently by minimum convex cost flow algorithms. The proposed algorithm decreases the objective function value monotonically in each iteration and terminates in a finite number of iterations.

The proposed method has several practical advantages. First, since the proposed method does not use Stirling’s approximation, it offers accurate inference even when the values in the count tables are small. This makes it possible to output solutions with much higher posterior probability than the approximation-based approach. Second, because the proposed method does not apply continuous relaxation, the obtained solution is guaranteed to be integer-valued, which results in sparse and interpretable outputs. Figure 1 illustrates the difference in the output of the proposed and existing methods. As shown, the output of the proposed method is integer-valued and sparse, while that of the existing method is not. In Section 4, we show results gained from synthetic and real-world datasets; they indicate that the proposed method outputs higher quality solutions than the existing approach. We show that the superiority of the proposed method is much greater when the overall population is not very large or the number of states on nodes in the graphical model is large.

2. Preliminaries

2.1. Collective Graphical Model (CGM)

Collective Graphical Model (CGM) is a probabilistic generative model that describes the distributions of aggregated statistics of multiple samples drawn from a certain graph-

ical model (Sheldon & Dietterich, 2011). Let $G = (V, E)$ be an undirected tree graph (i.e., a connected graph with no cycles) with $V = [N] := \{1, 2, \dots, N\}$. We consider a pairwise graphical model over discrete random variable $\mathbf{X} := (X_1, \dots, X_N)$ defined by

$$\Pr(\mathbf{X} = \mathbf{x}) = \frac{1}{Z} \prod_{(u,v) \in E} \phi_{u,v}(x_u, x_v),$$

where $\phi_{uv}(x_u, x_v)$ is a local potential function on edge (u, v) and $Z := \sum_{\mathbf{x}} \prod_{(u,v) \in E} \phi_{u,v}(x_u, x_v)$ is a partition function for normalization. In this paper, we assume that x_u takes values on the set $[R]$ for all $u \in V$.

We draw ordered samples $\mathbf{X}^{(1)}, \dots, \mathbf{X}^{(M)}$ independently from the graphical model. M is called the total population. We define *node contingency table* (count table) $\mathbf{n}_u := (n_u(i) \mid i \in [R])$ for $u \in V$ and *edge contingency table* $\mathbf{n}_{u,v} := (n_{u,v}(i, j) \mid i, j \in [R])$ for $(u, v) \in E$, which are the vectors whose entries are the number of occurrences of particular variable settings:

$$\begin{aligned} n_u(i) &:= \sum_{m=1}^M \mathbb{I}(X_u^{(m)} = i), \\ n_{u,v}(i, j) &:= \sum_{m=1}^M \mathbb{I}(X_u^{(m)} = i, X_v^{(m)} = j), \end{aligned}$$

where $\mathbb{I}(\cdot)$ is the indicator function. In CGM, observations $\mathbf{y} := ((\mathbf{y}_u)_{u \in V}, (\mathbf{y}_{u,v})_{(u,v) \in E})$ are generated by adding noise to contingency tables $\mathbf{n} := ((\mathbf{n}_u)_{u \in V}, (\mathbf{n}_{u,v})_{(u,v) \in E})$.

The MAP inference problem for CGM is to find \mathbf{n}^* which maximizes the posterior probability $\Pr(\mathbf{n}|\mathbf{y})$. Since $\Pr(\mathbf{n}|\mathbf{y}) = \Pr(\mathbf{n}, \mathbf{y}) / \Pr(\mathbf{y})$ from Bayes' rule, it suffices to maximize the joint probability $\Pr(\mathbf{n}, \mathbf{y}) = \Pr(\mathbf{n}) \cdot \Pr(\mathbf{y}|\mathbf{n})$, where $\Pr(\mathbf{y}|\mathbf{n})$ is the noise distribution associated with observation. $\Pr(\mathbf{n})$ is called CGM distribution and calculated as follows (Sun et al., 2015):

$$\Pr(\mathbf{n}) = F(\mathbf{n}) \cdot \mathbb{I}(\mathbf{n} \in \mathbb{L}_M^{\mathbb{Z}}), \quad (1)$$

$$\begin{aligned} F(\mathbf{n}) &:= \frac{M!}{Z^M} \cdot \frac{\prod_{u \in V} \prod_{i \in [R]} (n_u(i)!)^{\nu_u - 1}}{\prod_{(u,v) \in E} \prod_{i,j \in [R]} n_{u,v}(i,j)!} \\ &\quad \cdot \prod_{(u,v) \in E} \prod_{i,j \in [R]} \phi_{u,v}(i,j)^{n_{u,v}(i,j)}, \end{aligned} \quad (2)$$

$$\begin{aligned} \mathbb{L}_M^{\mathbb{Z}} &:= \left\{ \mathbf{n} \in \mathbb{Z}_{\geq 0}^{|V|R + |E|R^2} \mid M = \sum_{i \in [R]} n_u(i) \ (\forall u \in V), \right. \\ &\quad \left. n_u(i) = \sum_{j \in [R]} n_{u,v}(i,j) \ (\forall (u,v) \in E, i \in [R]) \right\}. \end{aligned} \quad (3)$$

Here, $\mathbb{L}_M^{\mathbb{Z}}$ is the set of contingency tables \mathbf{n} that satisfy the consistency of counts among the number of samples M ,

the node contingency tables \mathbf{n}_u , and the edge contingency tables $\mathbf{n}_{u,v}$. ν_u is the degree of node u in G . Using the above notations, the MAP inference problem can be written as

$$\min_{\mathbf{n} \in \mathbb{L}_M^{\mathbb{Z}}} -\log F(\mathbf{n}) - \log \Pr(\mathbf{y}|\mathbf{n}). \quad (4)$$

2.2. CGMs on Path Graphs

We explain the details of CGMs on path graphs, which is the main topic of this paper. Path graph P_n is an undirected graph whose vertex set is $V = [N]$ and edge set is $E = \{(t, t+1) \mid t \in [N-1]\}$. A graphical model (not CGM) on path graph is the most basic graphical model that represents a time series generated by a Markov model; that is, the current state depends only on the previous state. A CGM on a path graph represents the distribution of aggregated statistics when there are many individuals whose state transition is determined by a Markov model. In the rest of this paper, we use the notation $n_{ti} := n_t(i)$, $n_{tij} := n_{t,t+1}(i, j)$, and $\phi_{tij} := \phi_{t,t+1}(i, j)$ for simplicity.

To develop the concrete form of the MAP inference problem, we need to decide the observation model $\Pr(\mathbf{y}|\mathbf{n})$. In this paper, we consider the *node observation model*, a model in which observations are obtained at each node with independent noise. In this case, observation \mathbf{y} consists of y_{ti} ($t \in [N]$, $y \in [R]$), and its distribution is given by $\Pr(\mathbf{y}|\mathbf{n}) = \prod_{t \in [N]} \prod_{i \in [R]} p_{ti}(y_{ti}|n_{ti})$, where p_{ti} is the noise distribution. An additional assumption is described below.

Assumption 1. For $t \in [N]$ and $i \in [R]$, $\log p_{ti}(y|\mathbf{n})$ is a concave function in \mathbf{n} .

Assumption 1 is a quite common assumption in CGM studies (Sheldon et al., 2013; Sun et al., 2015). Commonly used noise distributions such as Gaussian distribution $p_{ij}(y_{ij}|t_{ij}) = \frac{1}{\sqrt{2\pi\sigma^2}} \exp\left(\frac{-(y_{ij}-t_{ij})^2}{2\sigma^2}\right)$ and Poisson distribution $p_{ij}(y_{ij}|t_{ij}) = \frac{t_{ij}^{y_{ij}} \cdot \exp(-t_{ij})}{y_{ij}!}$ satisfy Assumption 1. See Figure 2 for the relationship between these symbols.

We give an example drawn from human mobility. Consider a space that is divided into R distinct areas, and M people are moving around in the space. The time series of areas to which person m belongs at each time step, $\mathbf{X}^{(m)} = (X_1^{(m)}, \dots, X_N^{(m)})$, is determined by the graphical model $p(\mathbf{x}) = \frac{1}{Z} \prod_{t=1}^{N-1} \phi_{tx_t x_{t+1}}$. Here, $\phi_{tx_t x_{t+1}}$ is the affinity between two areas x_t and x_{t+1} at time step $t \rightarrow t+1$. n_{ti} represents the number of people in area i at time step t , and n_{tij} represents the number of people who moved from area i to area j at time step $t \rightarrow t+1$. We have noisy observations y_{ti} for $t \in [N]$ and $i \in [R]$, which are generated by adding noise to n_{ti} . The MAP inference problem we want to solve is to find the true population of each

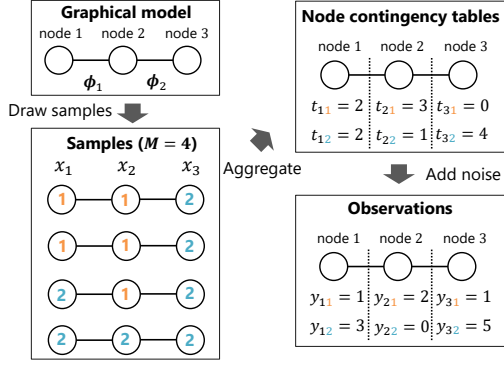


Figure 2. An example of generation process of observations in CGM on a path graph when $N = 3$, $R = 2$, $M = 4$.

area at each time step, $\{n_{ti}\}_{t \in [N], i \in [R]}$, and the true number of people moving between areas, $\{n_{tij}\}_{t \in [N-1], i, j \in [R]}$, with the highest posterior probability given the observation $\{y_{ti}\}_{t \in [N], i \in [R]}$.

From (1)–(4), the MAP inference problem for CGMs on path graphs can be written as follows:

$$\begin{aligned}
 \min_{\mathbf{n}} \quad & \sum_{t=1}^{N-1} \sum_{i, j \in [R]} f_{tij}(n_{tij}) + \sum_{t=2}^{N-1} \sum_{i \in [R]} g(n_{ti}) \\
 & + \sum_{t=1}^N \sum_{i \in [R]} h_{ti}(n_{ti}), \\
 \text{s.t.} \quad & \sum_{i \in [R]} n_{ti} = M \quad (t \in [N]), \\
 & \sum_{j \in [R]} n_{tij} = n_{ti} \quad (t \in [N-1], i \in [R]), \\
 & \sum_{i \in [R]} n_{tij} = n_{i+1, j} \quad (t \in [N-1], j \in [R]), \\
 & n_{tij}, n_{ti} \in \mathbb{Z}_{\geq 0},
 \end{aligned} \tag{5}$$

where

$$\begin{aligned}
 f_{tij}(z) &:= \log z! - z \cdot \log \phi_{tij}, \quad g(z) := -\log z!, \\
 h_{ti}(z) &:= -\log [p_{ti}(y_{ti}|z)].
 \end{aligned}$$

For the details of the derivation, please see Appendix. Let $\mathcal{P}(\mathbf{n})$ denote the objective function of problem (5).

3. Proposed Method

3.1. Formulation as Minimum Cost Flow Problem

First, we show that problem (5) can be formulated as the (non-linear) minimum cost flow problem (MCFP). MCFP is a combinatorial optimization problem on the directed graph $\mathcal{G} = (\mathcal{V}, \mathcal{E})$. Each node $i \in \mathcal{V}$ has a supply value $b_i \in \mathbb{Z}$, and each edge $(i, j) \in \mathcal{E}$ has a cost function $c_{ij} : \mathbb{Z}_{\geq 0} \rightarrow$

Algorithm 1 The MCFP instance construction algorithm

- 1: $\mathcal{V} := \{o, d\} \cup (\cup_{t \in [N]} (\mathcal{U}_t \cup \mathcal{W}_t))$, where $\mathcal{U}_t := \{u_{t,i}\}_{i \in [R]}$, $\mathcal{W}_t := \{w_{t,i}\}_{i \in [R]}$.
- 2: Add edge $(o, u_{1,i}, 0)$ for $i \in [R]$.
// $(u, v, c(z))$ represents an directed edge from node u to node v with cost function $c(z)$.
- 3: Add edge $(w_{N,i}, d, 0)$ for $i \in [R]$.
- 4: Add edge $(u_{t,i}, w_{t,i}, h_{ti}(z))$ for $t \in \{1, N\}$, $i \in [R]$.
- 5: Add edge $(u_{t,i}, w_{t,i}, g(z) + h_{ti}(z))$ for $t = 2, \dots, N-1$, $i \in [R]$.
- 6: Add edge $(w_{t,i}, u_{t+1,i}, f_{tij}(z))$ for $t \in [N-1]$, $i, j \in [R]$.
- 7: Set $b_o = M$, $b_d = -M$, $b_v = 0$ for $v \in \mathcal{V} \setminus \{o, d\}$.

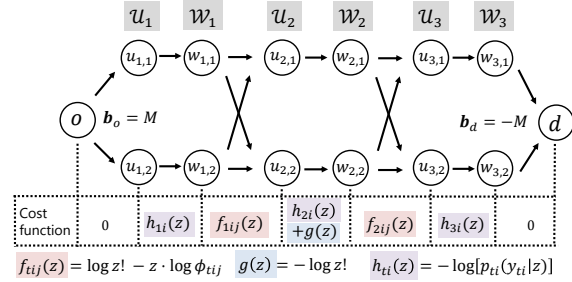


Figure 3. An MCFP instance constructed by Algorithm 1 when $N = 3$ and $R = 2$.

$\mathbb{R} \cup \{+\infty\}$. MCFP is the problem of finding a minimum cost flow on \mathcal{G} that satisfies the supply constraints at all nodes. MCFP can be described as follows:

$$\begin{aligned}
 \min_{\mathbf{z} \in \mathbb{Z}^{|\mathcal{E}|}} \quad & \sum_{(i,j) \in \mathcal{E}} c_{ij}(z_{ij}) \\
 \text{s.t.} \quad & \sum_{j: (i,j) \in \mathcal{E}} z_{ij} - \sum_{j: (j,i) \in \mathcal{E}} z_{ji} = b_i \quad (i \in \mathcal{V}).
 \end{aligned}$$

Note that \mathbf{z} takes only integer values (i.e., $\mathbf{z} \in \mathbb{Z}^{|\mathcal{E}|}$).

To formulate the MAP inference problem (5) as MCFP, we construct an MCFP instance by Algorithm 1.

Proposition 1. For \mathbf{n}^* defined by $n_{ti}^* := z_{u_{t,i}w_{t,i}}^*$ and $n_{tij}^* := z_{w_{t,i}u_{t+1,j}}^*$, where \mathbf{z}^* is an optimal solution of the MCFP instance constructed by Algorithm 1, \mathbf{n}^* is an optimal solution of problem (5).

Our proof is given in the Appendix. Figure 3 illustrates an example of an MCFP instance constructed by Algorithm 1 where $N = 3$ and $R = 2$. This MCFP can be interpreted as the problem of finding a way to push M flows from node o to node d with minimum cost.

3.2. Discrete convexity of cost functions

Proposition 1 implies that we can obtain the optimal solution of the MAP inference problem (5) by solving the MCFP

constructed above. This, however, is not an easy task.

In MCFP, the convexity of cost functions generally has a crucial impact on the computation complexity.

Definition 1. A function $f : \mathbb{Z}_{\geq 0} \rightarrow \mathbb{R} \cup \{+\infty\}$ is called a *discrete convex function* when $f(z+2) + f(z) \geq 2 \cdot f(z+1)$ for all $z \in \mathbb{Z}_{\geq 0}$. If $-f$ is a discrete convex function, f is called a *discrete concave function*.

A subclass of MCFP in which all cost functions are discrete convex functions is called the Minimum Convex Cost Flow Problem (C-MCFP); it is known to be efficiently solvable (Ahuja et al., 1993). However, the constructed MCFP is not an instance of C-MCFP.

Proposition 2. f_{tij} is a discrete convex function. Under Assumption 1, h_{ti} is a discrete convex function. g is a discrete concave function.

Proof is given in the Appendix. Thus, we cannot directly apply C-MCFP algorithms to our problem.

3.3. Application of DCA

To overcome this issue, we utilize the idea of the Difference of Convex Algorithm (DCA). We first explain the core idea of DCA based on the description in (Narasimhan & Bilmes, 2005). DCA is a general framework to solve the minimization problem $\min_{\mathbf{n} \in D} \mathcal{P}(\mathbf{n}) = \mathcal{Q}(\mathbf{n}) + \mathcal{R}(\mathbf{n})$, where $\mathcal{Q}(\mathbf{n})$ is a convex function and $\mathcal{R}(\mathbf{n})$ is a concave function. DCA does this by using the following procedure to generate a feasible solution sequence $\mathbf{n}^{(1)}, \dots, \mathbf{n}^{(s)}$ that satisfies $\mathcal{P}(\mathbf{n}^{(1)}) \geq \mathcal{P}(\mathbf{n}^{(2)}) \geq \dots \geq \mathcal{P}(\mathbf{n}^{(s)})$. First, we set an arbitrary feasible solution in D as $\mathbf{n}^{(1)}$. When we already have the sequence $\mathbf{n}^{(1)}, \dots, \mathbf{n}^{(s)}$, we find a function $\bar{\mathcal{R}}^{(s)}(\mathbf{n})$ that satisfies the following three conditions:

- (i) $\bar{\mathcal{R}}^{(s)}(\mathbf{n}^{(s)}) = \mathcal{R}(\mathbf{n}^{(s)})$,
- (ii) $\bar{\mathcal{R}}^{(s)}(\mathbf{n}) \geq \mathcal{R}(\mathbf{n}) \quad (\forall \mathbf{n} \in D)$,
- (iii) $\bar{\mathcal{P}}^{(s)}(\mathbf{n}) := \mathcal{Q}(\mathbf{n}) + \bar{\mathcal{R}}^{(s)}(\mathbf{n})$ can be minimized efficiently in D .

Because $\mathcal{R}(\mathbf{n})$ is concave, by setting $\bar{\mathcal{R}}^{(s)}(\mathbf{n}) = \mathcal{R}(\mathbf{n}^{(s)}) + \nabla \mathcal{R}(\mathbf{n}^{(s)}) \cdot (\mathbf{n} - \mathbf{n}^{(s)})$, which is a linear approximation of $\mathcal{R}(\mathbf{n})$ at $\mathbf{n}^{(s)}$, conditions (i)–(iii) hold. Using this function, we get a new feasible solution by $\mathbf{n}^{(s+1)} = \arg \min_{\mathbf{n}} \bar{\mathcal{P}}^{(s)}(\mathbf{n})$. This can be done easily because condition (iii) holds. Then, because $\mathcal{P}(\mathbf{n}^{(s+1)}) \leq \bar{\mathcal{P}}^{(s)}(\mathbf{n}^{(s+1)}) \leq \bar{\mathcal{P}}^{(s)}(\mathbf{n}^{(s)}) = \mathcal{P}(\mathbf{n}^{(s)})$, we get $\mathcal{P}(\mathbf{n}^{(1)}) \geq \mathcal{P}(\mathbf{n}^{(2)}) \geq \dots \geq \mathcal{P}(\mathbf{n}^{(s)}) \geq \mathcal{P}(\mathbf{n}^{(s+1)})$ by induction.

We apply the framework of DCA to our MAP inference problem. We decompose $\mathcal{P}(\mathbf{n})$, which is the objective function of (5), into $\mathcal{Q}(\mathbf{n}) = \sum_{t=1}^{N-1} \sum_{i,j \in [R]} f_{tij}(n_{tij}) +$

Algorithm 2 DCA for solving problem (5)

```

1:  $\mathbf{n}^{(1)} \leftarrow \mathbf{0}$ 
2: for  $s = 1, 2, \dots$  do
3:   for  $t = 2, \dots, N-1$  and  $i \in [R]$  do
4:     replace the cost function of edge  $(u_{t,i}, w_{t,i})$  in  $\mathcal{G}$ 
       by  $\bar{g}_{ti}^{(s)}(z) + h_{ti}(z)$ 
5:    $\mathbf{n}^{(s+1)} \leftarrow$  solve C-MCFP in  $\mathcal{G}$ 
6:   if  $\mathcal{P}(\mathbf{n}^{(s)}) = \mathcal{P}(\mathbf{n}^{(s+1)})$  then
7:     return  $\mathbf{n}^{(s)}$ 

```

$\sum_{t=1}^N \sum_{i \in [R]} h_{ti}(n_{ti})$ and $\mathcal{R}(\mathbf{n}) = \sum_{t=2}^{N-1} \sum_{i \in [R]} g(n_{ti})$, and let D be the feasible region of (5).

Proposition 3. Let $\bar{g}_{ti}^{(s)}(z) := -\log(n_{ti}^{(s)}!) + \alpha_{ti}^{(s)} \cdot (z - n_{ti}^{(s)})$, where $\alpha_{ti}^{(s)}$ is a real number which satisfies $-\log(n_{ti}^{(s)} + 1) \leq \alpha_{ti}^{(s)} \leq -\log n_{ti}^{(s)}$. Then, the function $\bar{\mathcal{R}}^{(s)}(\mathbf{n}) := \sum_{t=2}^{N-1} \sum_{i \in [R]} \bar{g}_{ti}^{(s)}(n_{ti})$ satisfies $\bar{\mathcal{R}}^{(s)}(\mathbf{n}^{(s)}) = \mathcal{R}(\mathbf{n}^{(s)})$ and $\bar{\mathcal{R}}^{(s)}(\mathbf{n}) \geq \mathcal{R}(\mathbf{n})$.

Please see the Appendix for the proof. Proposition 3 says that the function $\bar{\mathcal{R}}^{(s)}(\mathbf{n})$ satisfies conditions (i) and (ii). Intuitively, $\bar{g}_{ti}^{(s)}(\mathbf{n})$ is a tangent of g at n_{ti} .

We check condition (iii). We consider the MCFP instance constructed by Algorithm 1. Then, we slightly modify this instance by changing the cost function of edge $(u_{t,i}, w_{t,i})$ from $g(z) + h_{ti}(z)$ to $\bar{g}_{ti}^{(s)}(z) + h_{ti}(z)$ for $t = 2, \dots, N-1$, $i \in [R]$. It can be easily verified that the minimization problem of $\bar{\mathcal{P}}^{(s)}(\mathbf{n})$ in D is equivalent to solving this new MCFP instance. Because all the cost functions on edges satisfy discrete convexity in this new MCFP instance, we can solve it efficiently by applying existing algorithms for C-MCFP. (The details are discussed in Section 3.4.)

From above arguments, we can construct an efficient optimization algorithm for the MAP inference problem (5) by applying the DCA framework to our problem. An overall view of the derived algorithm is given in Algorithm 2. The algorithm is guaranteed to terminate after a finite number of iterations because $\mathcal{P}(\mathbf{n}^{(s)})$ monotonically decreases and D is a finite set.

3.4. Time complexity of one iteration

We analyze the time complexity of one iteration of the proposed method (Lines 3–7 in Algorithm 2). The computation bottleneck is solving C-MCFP in \mathcal{G} (Line 5). There are several algorithms to solve C-MCFP and time complexity varies depending on which one is adopted. In this paper, we consider two typical methods, Successive Shortest Path (SSP) and Capacity Scaling (CS) (Ahuja et al., 1993).

For C-MCFP with Graph $\mathcal{G} = (\mathcal{V}, \mathcal{E})$ and total flow M , the time complexity of SSP is $O(M|\mathcal{E}| \log |\mathcal{V}|)$ and that

Table 1. Attained objective functions in synthetic instances. For each setting, we generated 10 instances and average values are shown. The smallest value is highlighted for each setting. U and D mean the “uniform” and “distance” potential setting, respectively.

M		10^1			10^2			10^3		
		10	20	30	10	20	30	10	20	30
U	Proposed (L)	-9.97e+01	-8.90e+01	-8.74e+01	-1.11e+03	-1.19e+03	-1.22e+03	-1.07e+04	-1.31e+04	-1.40e+04
	Proposed (M)	-9.81e+01	-8.90e+01	-8.74e+01	-1.11e+03	-1.19e+03	-1.22e+03	-1.07e+04	-1.31e+04	-1.40e+04
	Proposed (R)	-9.64e+01	-8.76e+01	-8.74e+01	-1.11e+03	-1.18e+03	-1.21e+03	-1.07e+04	-1.31e+04	-1.40e+04
	NLBP	-7.19e+01	-7.01e+01	-7.01e+01	-1.08e+03	-9.87e+02	-9.02e+02	-1.07e+04	-1.30e+04	-1.37e+04
D	Proposed (L)	3.35e-01	5.00e-01	5.00e-01	-5.48e+01	-3.03e+01	-1.18e+01	-5.83e+00	-9.06e+02	-1.01e+03
	Proposed (M)	3.35e-01	5.00e-01	5.00e-01	-5.43e+01	-2.91e+01	-1.14e+01	-5.82e+00	-9.06e+02	-1.01e+03
	Proposed (R)	3.35e-01	5.00e-01	5.00e-01	-5.39e+01	-2.89e+01	-1.06e+01	-5.80e+00	-9.06e+02	-1.01e+03
	NLBP	3.20e+01	4.56e+01	5.28e+01	-1.38e+01	1.77e+02	3.25e+02	1.20e+00	-8.02e+02	-5.31e+02

of CS is $O(|\mathcal{E}|^2 \log |\mathcal{V}| \log M)$. Because $|\mathcal{V}| = O(NR)$ and $|\mathcal{E}| = O(NR^2)$ in our problem, time complexity in one iteration is $O(MNR^2 \log(NR))$ when SSP is applied and $O(N^2R^4 \log(NR) \log M)$ when CS is applied. This result implies that each method has its own advantages and disadvantages: SSP has small computation complexity for N and R , while CS has small computation complexity for M . This difference is confirmed empirically in Section 4.1.

4. Experiments

We perform experiments to evaluate the effectiveness of the proposed method using synthetic and real-world instances. All experiments are conducted on a 64-bit macOS machine with Intel Core i7 CPUs and 16 GB of RAM. All algorithms are implemented in C++ (gcc 9.1.0 with -O3 option).

4.1. Synthetic Instances

Settings. We solve randomly generated synthetic instances of the MAP inference problem (5). We fix T to 5 and vary the values of R and M . The input observation y_{ti} is independently drawn from uniform distribution on the set of integers $\{1, 2, \dots, 2 \cdot \lfloor \frac{M}{R} \rfloor\}$. As the noise distribution, we use Gaussian distribution $p_{ij}(y_{ij}|t_{ij}) \propto \exp\left(\frac{-(y_{ij}-t_{ij})^2}{100}\right)$. We use two types of potential functions as follows. (1) **uniform.** ϕ_{tij} is independently drawn from uniform distribution on the set of integers $\{1, 2, \dots, 10\}$. (2) **distance.** We set $\phi_{tij} = \frac{1}{|i-j+1|}$. This potential models the movement of individuals in one-dimensional space: the state indices i and j represent coordinates in the space, and the closer the two points are, the more likely are movements between them to occur.

Proposed Method. To construct surrogate functions in the proposed method, we can choose arbitrary $\alpha_{ti}^{(s)}$ which satisfies the condition $-\log(n_{ti}^{(s)} + 1) \leq \alpha_{ti}^{(s)} \leq -\log n_{ti}^{(s)}$ (see Proposition 3). To investigate the influence of the choice of $\alpha_{ti}^{(s)}$, we try three strategies to decide $\alpha_{ti}^{(s)}$: (1) $\alpha_{ti}^{(s)} = -\log(n_{ti}^{(s)})$, (2) $\alpha_{ti}^{(s)} = -\frac{1}{2}(\log(n_{ti}^{(s)}) + \log(n_{ti}^{(s)} + 1))$, (3) $\alpha_{ti}^{(s)} = -\log(n_{ti}^{(s)} + 1)$. We call them Proposed (L),

Proposed (M), Proposed (R), respectively.

Compared Method. As the compared method, we use Non-Linear Belief Propagation (NLBP) (Sun et al., 2015), which is a message-passing style algorithm to solve approximate MAP inference problem derived by applying Stirling’s approximation and continuous relaxation. Because the output of NLBP is not integer-valued and $\log(z!)$ is defined only if z is an integer, we cannot calculate the objective function of (5) directly. To address this, we calculate it by replacing the term $\log(z!)$ by linear interpolation of $\log(\lfloor z \rfloor!)$ and $\log(\lceil z \rceil!)$, which is given by $(\lceil z \rceil - z) \cdot \log(\lfloor z \rfloor!) + (z - \lfloor z \rfloor) \cdot \log(\lceil z \rceil!)$. Note that although there are various algorithms to solve the approximate MAP inference problem (see Section 5.1), the objective function values attained by these algorithms are the same. This is because the approximate problem is a convex optimization problem (Sheldon et al., 2013).

Comparison of attained objective values. The results are shown in Table 1. We generated 10 instances for each parameter setting and determined the average of attained objective function values. Because the objective function $\mathcal{P}(\mathbf{n})$ is equal to $-\log \Pr(\mathbf{n}|\mathbf{y}) + \text{const.}$, $\mathcal{P}(\mathbf{n})$ takes both positive and negative values, and the difference of the objective function values is essential; when $\mathcal{P}(\mathbf{n}_1) - \mathcal{P}(\mathbf{n}_2) = \delta$, $\Pr(\mathbf{n}_1|\mathbf{y}) = \exp(-\delta) \cdot \Pr(\mathbf{n}_2|\mathbf{y})$ holds.

All the proposed methods consistently have smaller objective function values than the compared method. The difference tends to be large when R is large and M is small. This would be because small values appear in the contingency table more frequently when R is large and M is small, and the effect of the inaccuracy of Stirling’s approximation becomes larger. Among three proposed methods, there was not much difference in obtained objective function values, but Proposed (L) was found to consistently achieve slightly smaller objective function values than others.

Characteristics of the output solution. To compare the characteristics of solutions obtained by proposed (L) and NLBP, we solve two instances (1) $R = 20$, $M = 10^2$, uniform potential (2) $R = 20$, $M = 10^2$, distance potential by

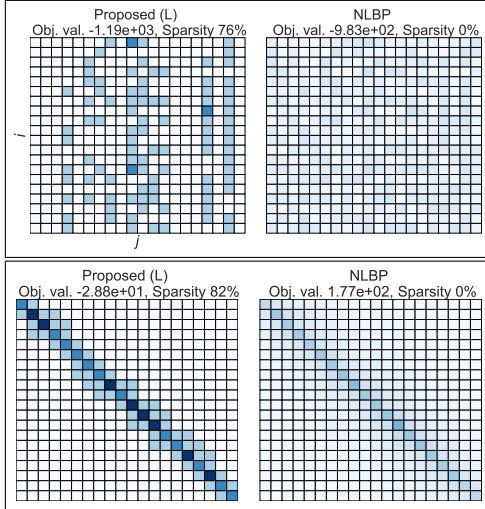


Figure 4. Comparison of solutions yielded by proposed method (L) and NLBP. We solve two instances with $R = 20$, $M = 10^2$ and uniform potential (top) and $R = 20$, $M = 10^2$ and distance potential (bottom). The obtained edge contingency table n_{1ij} is presented as a matrix heatmap with maximum value of color map 3. For both potential settings, the solution by the proposed method is quite sparse while that by NLBP contains a lot of non-zero elements.

each method. Obtained edge contingency tables n_{1ij} are shown in Figure 4 as heat maps. For both potential settings, proposed method outputs sparse solutions while the solutions by NLBP are blurred and contain a lot of non-zero elements. This difference is quantified by “sparsity”, which is calculated by $1.0 - (\# \text{ of non-zero } (> 10^{-2}) \text{ elements}) / (\# \text{ of elements})$: sparsity of the output of proposed (L) is 76% (uniform potential), 83% (distance potential), while the sparsity of the output of NLBP is 0% in both settings. This is caused by its application of continuous relaxation and the inaccuracy of Stirling’s approximation around 0. In additional experiments, we observed that the output of the two methods become closer as M increases. For more details, please see the Appendix.

Comparison of computation time. We compare the computation time of each algorithm. As explained in Section 3.4, we can choose an arbitrary C-MCFP algorithm as the subroutine in the proposed method and the time complexity varies depending on the choice. We compare proposed (L) with SSP, proposed (L) with CS, and NLBP.

Figure 5 shows the relationship between input size and computation time, and Figure 6 shows the relationship between running time and objective function value. These results are consistent with the complexity analysis results in Section 3.4; SSP is efficient when R is large but becomes inefficient when M is large, and the converse is true for CS. The results also suggest that it is important to choose the algorithm

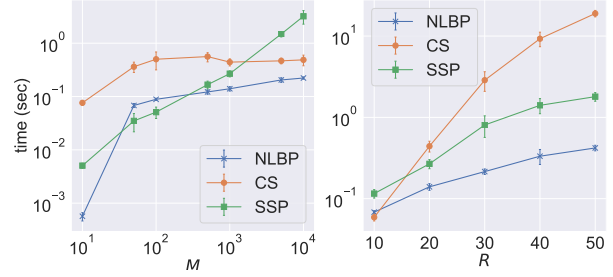


Figure 5. The average computation time of each algorithm. The values are averages of 10 synthetic instances when R is fixed to 20 (left) an M is fixed to 10^3 (right). N is set 5 and uniform potential is used. The error bars represent standard deviations.

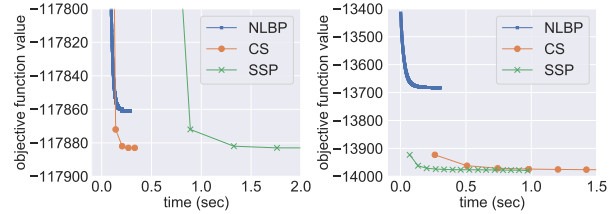


Figure 6. The relationship between running time and objective function value. The left figure shows the result of an instance of $R = 20$, $M = 10^4$ and uniform potential, and right figure shows that of $R = 30$, $M = 10^3$ and uniform potential.

depending on the size parameter of the input. The proposed method is not much worse than the existing method in terms of computation time by choosing an appropriate C-MCFP algorithm according to the size of the input. Appropriately chosen proposed methods attain the minimum of the existing method more quickly; proposed methods take a lot of time to achieve a smaller objective function value than the minimum of the existing method.

4.2. Real-world Instances

We conduct experiments using real-world population datasets. The datasets are generated from 8694 car trajectories collected by a car navigation application in the Greater Tokyo area, Japan¹. We randomly sample M ($M = 10^1, 10^2, 10^3$) trajectories from this data and create aggregated population data of each area at fixed time intervals. The areas are decided by dividing the targeted geospatial space into fixed size grid cells. The grid size is set to $10\text{km} \times 10\text{km}$ ($R = 8 \times 7 = 56$) and $5\text{km} \times 5\text{km}$ ($R = 16 \times 13 = 208$), and time interval is 60 minutes ($N = 24$). We construct the potential $\phi_{tij} = \frac{1}{1 + \text{dist}(i,j)}$, where $\text{dist}(i,j)$ is the Euclidean distance between the centers of cell i and cell j in the grid space. We created 10

¹We use the car data collected by the smartphone car navigation application of NAVITIME JAPAN Co., Ltd. (<http://corporate.navitime.co.jp/en/>)

Table 2. Attained objective functions for real-world instances. For each setting, we generated 10 instances and average values are shown. The smallest value is highlighted for each setting.

M	10^1		10^2		10^3	
	56	208	56	208	56	208
Proposed (L)	2.30e+00	2.30e+00	-1.26e+03	2.31e+01	-2.22e+04	-2.22e+04
Proposed (M)	2.30e+00	2.30e+00	-1.25e+03	2.31e+01	-2.22e+04	-2.22e+04
Proposed (R)	2.30e+00	2.30e+00	-1.20e+03	2.31e+01	-2.20e+04	-2.21e+04
NLBP	2.76e+02	3.83e+02	1.91e+03	3.85e+03	-1.47e+04	1.73e+04

instances by random sampling and averaged the attained objective function values for each setting.

Table 2 shows the results. The trends are similar to those found in experiments on synthetic instances: (i) Proposed methods consistently attain smaller objective values than the existing method. (ii) Superiority of the proposed method increase when R is large and M is small. (iii) Proposed (L) attains the best score among the proposed methods, but the difference is relatively small.

5. Related Work

5.1. MAP inference for CGMs

Several methods have been proposed for the MAP inference of CGMs, but most of them take the approach of solving the approximate problem (Sheldon et al., 2013), which is derived by applying Stirling’s approximation and continuous relaxation. For example, the interior point method (Sheldon et al., 2013), projected gradient descent (Vilnis et al., 2015), message passing (Sun et al., 2015) and Sinkhorn-Knopp algorithm (Singh et al., 2020) have been used to solve the approximate problem. In particular, (Nguyen et al., 2016) proposes a method to use DCA to solve this approximate problem. Although this approach is similar to our proposal in that it uses DCA, the purpose of applying DCA is totally different: our focus is to solve the MAP inference problem without using any approximation or continuous relaxation.

One of the few exceptions is the method proposed in (Akagi et al., 2020), which solves the original MAP inference problem directly without using approximation. Our method follows this line of research, but there are two major differences. First, their method can only be applied to CGM on a graph with two vertices, and thus applicability is very limited. Since our method is consistent with this method when applied to CGM on a graph with two vertices, our method can be regarded as a generalization of their method. Second, their work assumes accurate observations and so does not mention how to handle observation noise.

(Sheldon et al., 2007) solves related collective MAP inference problems on path graphs. The problems addressed in this paper are different from ours; their purpose is finding the most likely assignments of the entire variables for each individual, while our purpose is finding the most likely node

and edge contingency tables. In their settings, non-linear terms in the log posterior probability vanish, and the MAP inference problem can be solved easily by linear optimization approaches.

5.2. Difference of Convex Algorithm (DCA)

DCA, which is sometimes called Convex Concave Procedure (Yuille & Rangarajan, 2001), is a framework to minimize a function expressed as the sum of a convex function and a concave function (Le Thi & Dinh, 2018). DCA was originally proposed as a method for optimization in continuous domains. DCA has been used in various machine learning fields, such as feature selection (Le Thi et al., 2015), reinforcement learning (Piot et al., 2014), support vector machines (Xu et al., 2017) and Boltzmann machines (Nitanda & Suzuki, 2017).

Several studies have applied DCA to discrete optimization problems. This line of research is sometimes called discrete DCA (Maehara & Murota, 2015). (Narasimhan & Bilmes, 2005; Iyer & Bilmes, 2012) propose algorithms to minimize the sum of a submodular function and a supermodular function. This algorithm is generalized to yield the minimization of the sum of an M/L-convex function and an M/L-concave function (Maehara & Murota, 2015), where M-convex function and L-convex function are classes of discrete convex functions (Murota, 1998). Although our work is closely related to these studies, it is not part of them. This is because our problem can be regarded as the minimization of the sum of two M-convex functions and a separable concave function, and this is not included in the class of functions dealt with in (Maehara & Murota, 2015)².

6. Conclusion

In this paper, we propose a non-approximate method to solve the MAP inference problem for CGMs on path graphs. Our algorithm is based on an MCFP formulation and application of DCA. In the algorithm, surrogate functions can be constructed in closed-form and minimized efficiently by C-MCFP algorithms. Experimental results show that our al-

²A separable convex function is both L-convex and M-convex, but a sum of two M-convex functions is neither M-convex nor L-convex.

gorithm outperforms approximation-based methods in terms of quality of solutions.

References

- Ahuja, R. K., Magnanti, T. L., and Orlin, J. B. *Network Flows: Theory, Algorithms, and Applications*. Prentice-Hall, Inc., 1993.
- Akagi, Y., Nishimura, T., Kurashima, T., and Toda, H. A fast and accurate method for estimating people flow from spatiotemporal population data. In *IJCAI*, pp. 3293–3300, 2018.
- Akagi, Y., Nishimura, T., Tanaka, Y., Kurashima, T., and Toda, H. Exact and efficient inference for collective flow diffusion model via minimum convex cost flow algorithm. In *AAAI*, pp. 3163–3170, 2020.
- Du, J., Kumar, A., and Varakantham, P. On understanding diffusion dynamics of patrons at a theme park. In *AAMAS*, pp. 1501–1502, 2014.
- Iyer, R. and Bilmes, J. Algorithms for approximate minimization of the difference between submodular functions, with applications. In *UAI*, pp. 407–417, 2012.
- Le Thi, H. A. and Dinh, T. P. DC programming and DCA: Thirty years of developments. *Mathematical Programming*, 169(1):5–68, 2018.
- Le Thi, H. A., Le, H. M., and Dinh, T. P. Feature selection in machine learning: an exact penalty approach using a difference of convex function algorithm. *Machine Learning*, 101(1):163–186, 2015.
- Maehara, T. and Murota, K. A framework of discrete DC programming by discrete convex analysis. *Mathematical Programming*, 152(1-2):435–466, 2015.
- Morimura, T., Osogami, T., and Idé, T. Solving inverse problem of Markov chain with partial observations. In *NIPS*, pp. 1655–1663, 2013.
- Murota, K. Discrete convex analysis. *Mathematical Programming*, 83(1):313–371, 1998.
- Narasimhan, M. and Bilmes, J. A submodular-supermodular procedure with applications to discriminative structure learning. In *UAI*, pp. 404–412, 2005.
- Nguyen, T., Kumar, A., Lau, H. C., and Sheldon, D. Approximate inference using DC programming for collective graphical models. In *AISTATS*, pp. 685–693, 2016.
- Nitanda, A. and Suzuki, T. Stochastic difference of convex algorithm and its application to training deep Boltzmann machines. In *AISTATS*, pp. 470–478. PMLR, 2017.
- Piot, B., Geist, M., and Pietquin, O. Difference of convex functions programming for reinforcement learning. In *NIPS*, pp. 2519–2527, 2014.
- Sheldon, D., Elmohamed, M. S., and Kozen, D. Collective inference on Markov models for modeling bird migration. In *NIPS*, pp. 1321–1328, 2007.
- Sheldon, D., Sun, T., Kumar, A., and Dietterich, T. Approximate inference in collective graphical models. In *ICML*, pp. 1004–1012, 2013.
- Sheldon, D. R. and Dietterich, T. G. Collective graphical models. In *NIPS*, pp. 1161–1169, 2011.
- Singh, R., Haasler, I., Zhang, Q., Karlsson, J., and Chen, Y. Inference with aggregate data: An optimal transport approach. 2020. arXiv:2003.13933.
- Sun, T., Sheldon, D., and Kumar, A. Message passing for collective graphical models. In *ICML*, pp. 853–861, 2015.
- Suzuki, T., Yamashita, M., and Terada, M. Using mobile spatial statistics in field of disaster prevention planning. *NTT DOCOMO Tech. J.*, 14(3):37–45, 2013.
- Tanaka, Y., Tanaka, T., Iwata, T., Kurashima, T., Okawa, M., Akagi, Y., and Toda, H. Spatially aggregated gaussian processes with multivariate areal outputs. In *NeurIPS*, pp. 3000–3031, 2019.
- Terada, M., Nagata, T., and Kobayashi, M. Population estimation technology for mobile spatial statistics. *NTT DOCOMO Technical Journal*, 14(3):10–15, 2013.
- Vilnis, L., Belanger, D., Sheldon, D., and McCallum, A. Bethe projections for non-local inference. In *UAI*, pp. 892–901, 2015.
- Xu, H.-M., Xue, H., Chen, X.-H., and Wang, Y.-Y. Solving indefinite kernel support vector machine with difference of convex functions programming. In *AAAI*, pp. 2782–2788, 2017.
- Yuille, A. L. and Rangarajan, A. The concave-convex procedure (CCCP). In *NIPS*, pp. 1033–1040, 2001.
- Zhang, S., Wu, G., Costeira, J. P., and Moura, J. M. Understanding traffic density from large-scale web camera data. In *CVPR*, pp. 5898–5907, 2017.
- Zhang, Y., Charoenphakdee, N., Wu, Z., and Sugiyama, M. Learning from aggregate observations. In *NeurIPS*, pp. 470–478, 2020.

Appendices

A. Derivation of (5)

Because

$$\nu_t = \begin{cases} 1 & \text{if } t = 1, N, \\ 2 & \text{otherwise} \end{cases}$$

holds on path graphs, we have

$$F(\mathbf{n}) = \frac{M!}{Z^M} \cdot \frac{\prod_{t=2}^{N-1} \prod_{i \in [R]} n_{ti}!}{\prod_{t=1}^{N-1} \prod_{i,j \in [R]} n_{tij}!} \cdot \prod_{t=1}^{N-1} \prod_{i,j \in [R]} \phi_{tij}^{n_{tij}}$$

from (2). This gives

$$\begin{aligned} & -\log F(\mathbf{n}) - \log \Pr(\mathbf{y}|\mathbf{n}) \\ &= -\log M! + M \log Z \\ & - \sum_{t=2}^{N-1} \sum_{i \in [R]} \log n_{ti}! + \sum_{t=1}^{N-1} \sum_{i,j \in [R]} \log n_{tij}! \\ & - \sum_{t=1}^{N-1} \sum_{i,j \in [R]} n_{tij} \log \phi_{tij} - \sum_{t=1}^N \sum_{i \in [R]} \log p_{ti}(\mathbf{y}|\mathbf{n}) \\ &= \sum_{t=1}^{N-1} \sum_{i,j \in [R]} f_{tij}(n_{tij}) + \sum_{t=2}^{N-1} \sum_{i \in [R]} g(n_{ti}) \\ & + \sum_{t=1}^N \sum_{i \in [R]} h_{ti}(n_{ti}) + C, \end{aligned}$$

where C is a constant. We can verify easily that the feasible region of problem (5) is \mathbb{L}_M^Z defined in (3).

B. Proofs

B.1. Proof of Proposition 1

Proof. There is a one-to-one correspondence between a feasible solution to problem (5), \mathbf{n} , and a feasible solution to the MCFP instance constructed by Algorithm 1, \mathbf{z} , under the relationship $n_{ti} = z_{u_t, i} w_{t, i}$ and $n_{tij} = z_{w_t, i} u_{t+1, j}$; the constraint $\sum_{i \in [R]} n_{ti} = M$ is equivalent to the supply constraints at node o and d , the constraint $\sum_{j \in [R]} n_{tij} = n_{ti}$ corresponds to the flow conservation rule at node $w_{t, i}$ and the constraint $\sum_{i \in [R]} n_{tij} = n_{i+1, j}$ corresponds to the flow conservation rule at node $u_{t+1, j}$. Moreover, corresponding \mathbf{n} and \mathbf{z} and have the same objective function value in problem (5) and the MCFP instance, respectively. These facts yield the Proposition. \square

B.2. Proof of Proposition 2

Proof. The function $\log z!$ is a discrete convex function, since

$$\begin{aligned} & \log(z+2)! + \log z! - 2 \log(z+1)! \\ &= \log(z+2) - \log(z+1) \geq 0. \end{aligned}$$

This yields that $f_{tij}(z) = \log z! - z \cdot \log \phi_{tij}$ is a discrete convex function and $g(z) = -\log z!$ is a discrete concave function. Because a univariate continuous convex function is also a discrete convex function, $h_{ti}(z) = -\log [p_{ti}(\mathbf{y}_{ti}|z)]$ is a discrete convex function from Assumption 1. \square

B.3. Proof of Proposition 3

Proof. First, we show that

$$-\log(w!) + \alpha \cdot (z - w) \geq -\log(z!), \quad \forall z \in \mathbb{Z}_{\geq 0} \quad (6)$$

holds for arbitrary $w \in \mathbb{Z}_{\geq 0}$, when $-\log(w+1) \leq \alpha \leq -\log w$. When $z \geq w$,

$$\begin{aligned} & -\log(w!) + \alpha \cdot (z - w) + \log(z!) \\ &= \sum_{k=w+1}^z (\alpha + \log k) \geq 0 \end{aligned}$$

holds because $\alpha + \log(w+1) \geq 0$. When $z < w$,

$$\begin{aligned} & -\log(w!) + \alpha \cdot (z - w) + \log(z!) \\ &= \sum_{k=z+1}^w (-\alpha - \log k) \geq 0 \end{aligned}$$

holds because $-\alpha - \log w \geq 0$. Thus, inequality (6) holds.

Substituting $w = n_{ti}^{(s)}$ in (6), we get $\bar{g}_{ti}^{(s)}(z) \geq g(z)$ for all $z \in \mathbb{Z}_{\geq 0}$. This yields

$$\bar{\mathcal{R}}^{(s)}(\mathbf{n}) = \sum_{t=2}^{N-1} \sum_{i=1}^R \bar{g}_{ti}^{(s)}(n_{ti}) \geq \sum_{t=2}^{N-1} \sum_{i=1}^R g(n_{ti}) = \mathcal{R}(\mathbf{n}).$$

Furthermore, since $\bar{g}_{ti}^{(s)}(n_{ti}^{(s)}) = g(n_{ti}^{(s)})$ from simple calculation, we get $\bar{\mathcal{R}}^{(s)}(\mathbf{n}^{(s)}) = \mathcal{R}(\mathbf{n}^{(s)})$. \square

C. Additional experimental results

C.1. The Characteristics of the solutions

We run the same experiments as Figure 4 varying the value of M . The results are shown in Figures 7 and 8. The outputs

of the two methods are totally different when M is small, and they get closer as M increases. This is owing to the nature of Stirling’s approximation $\log x! \approx x \log x - x$; it is inaccurate especially when x is small.

C.2. Histogram interpolation

As an application of MAP inference of CGMs on path graphs, we can interpolate the time series of histograms between given two histograms. In this section, we show experimental results on this application and discuss the differences between the output of the proposed method and that of the existing method.

C.2.1. SETTINGS

First, we briefly explain how to realize interpolation between two histograms by MAP inference of CGMs on path graphs. Suppose we are given histogram $\boldsymbol{\eta}_1 := [\eta_{11}, \dots, \eta_{1R}]$ at time 1 and the histogram $\boldsymbol{\eta}_N := [\eta_{N1}, \dots, \eta_{NR}]$ at time N . The interpolated histogram $\boldsymbol{\eta}_t$ at time t ($= 2, \dots, N - 1$) is calculated by the following procedure.

1. Consider a CGM on a path graph with N vertices.
2. Let $\mathbf{y}_1 = \boldsymbol{\eta}_1$ and $\mathbf{y}_N = \boldsymbol{\eta}_N$.
3. \mathbf{y}_t ($t = 2, \dots, N - 1$) is treated as a *missing value*. This can be achieved by setting $h_{ti}(z) = 0$ ($t = 2, \dots, N - 1, i \in [R]$) in the objective function of the problem (5).
4. Find a solution \mathbf{n}^* to the MAP inference problem under an appropriate potential ϕ .
5. Obtain an interpolation result by $\eta_{ti} = n_{ti}^*$ ($t = 2, \dots, N - 1, i \in [R]$).

In our experiment, we consider a grid space of size $5 \times 5 = 25$ ($= R$) and a histogram $\boldsymbol{\eta} := [\eta_1, \dots, \eta_R]$ with a value η_i for each cell i ($= 1, \dots, R$). To get interpolation results which consider the geometric structure defined by Euclidean distance in grid space, we set the potential $\phi_{tij} = \exp(-((x_i - x_j)^2 + (y_i - y_j)^2))$, where (x_i, y_i) is the two-dimensional coordinate of the center of cell i in the grid space. We set $N = 6$ and use Gaussian distribution $p_{ij}(y_{ij}|n_{ij}) \propto \exp(-5(y_{ij} - n_{ij})^2)$ for the noise distributions at $t = 1, N$.

C.2.2. RESULTS

The results are shown in Figure 9. Note that Figure 9 illustrates different objects from what is shown in Figures 4, 7 and 8; Figure 9 illustrates the interpolated node contingency table values n_{ti} as two-dimensional grid spaces, while Figures 7 and 8 illustrate edge contingency table values n_{tij}

as matrices. As shown in the figure, NLBP tends to assign non-zero values to many cells, while proposed (L) assigns non-zero values to a small number of cells, resulting in sparse solutions. Moreover, the outputs of the proposed (L) are integer-valued while those of NLBP are not. This characteristic of the proposed method is beneficial for interpretability when the histogram values are the numbers of countable objects (e.g., the number of people in the area).

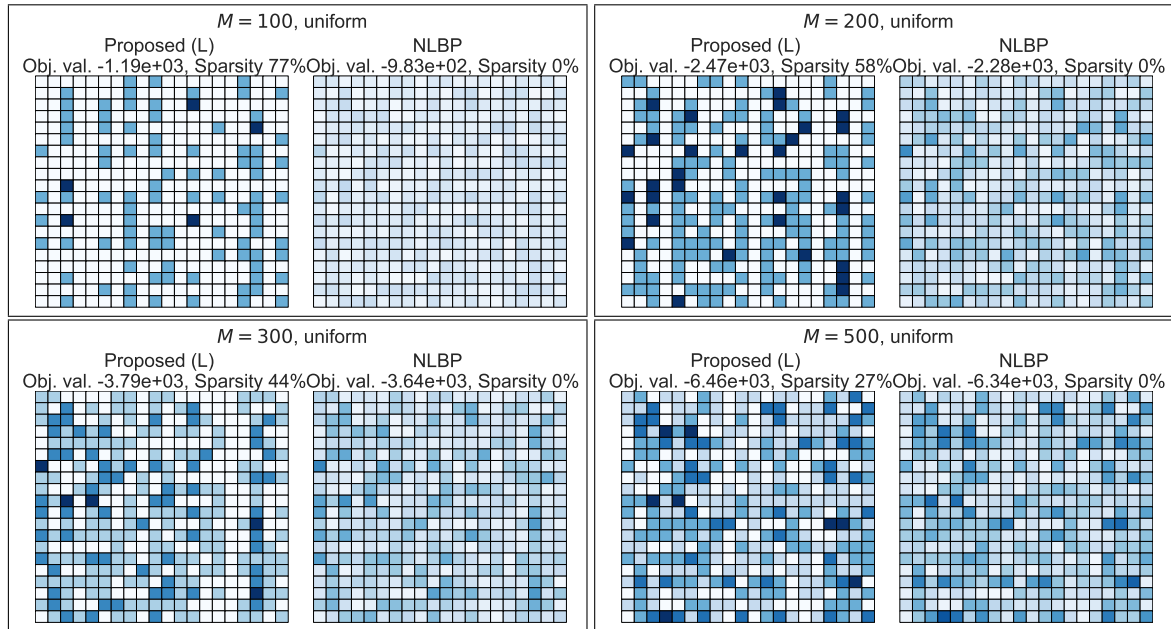


Figure 7. Comparison of solutions yielded by the proposed method (L) and NLBP when $R = 20$ and the uniform potential is used.

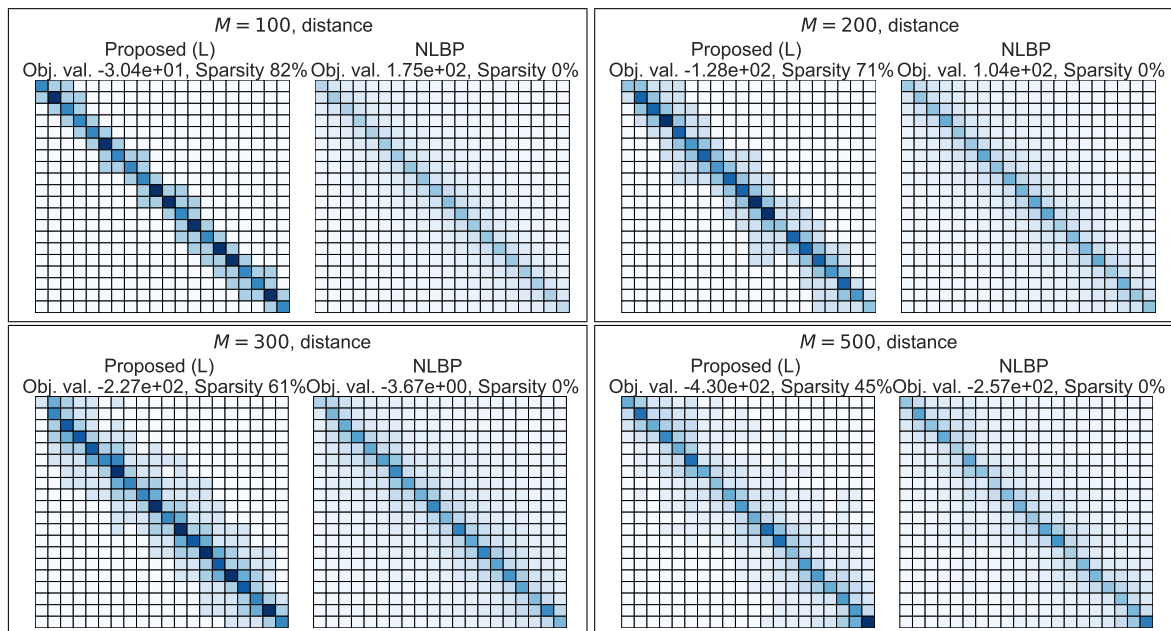


Figure 8. Comparison of solutions yielded by the proposed method (L) and NLBP when $R = 20$ and the distance potential is used.

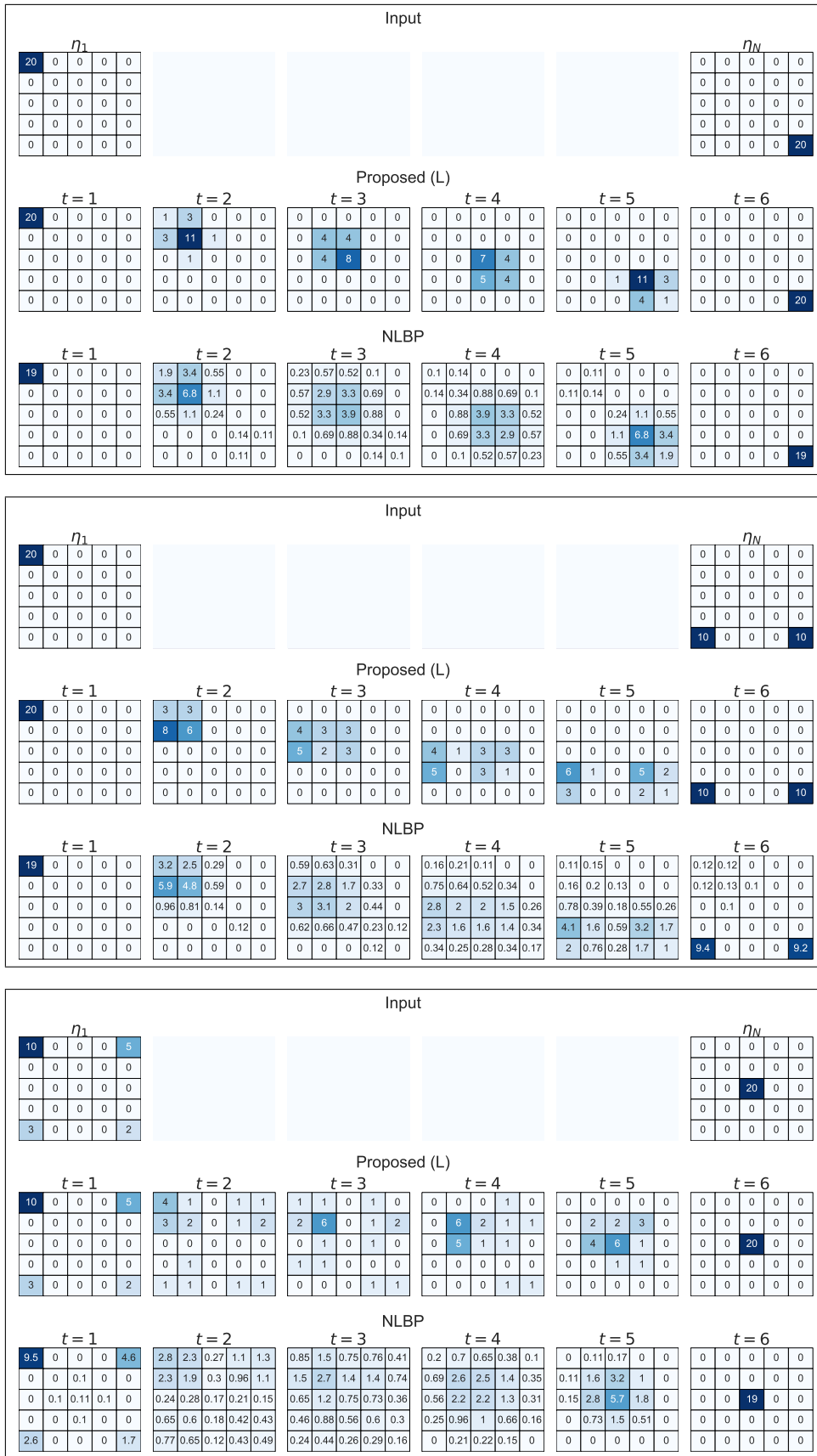


Figure 9. Three examples of interpolation results yielded by each method. In each example, three sequences of histograms in the two-dimensional grid space are presented; the first row shows the input histograms η_1 and η_N , the second row shows the interpolation results obtained by proposed (L), and the third row shows the interpolation results obtained by NLBP. Note that the values smaller than 10^{-2} are rounded for visibility.